IEEE Photonics Journal
An IEEE Photonics Society Publication

Open Access

Tunable Vernier Microring Optical Filters With $p-i-p$-Type Microheaters

Volume 5, Number 4, August 2013

Linjie Zhou, Member, IEEE
Xiaoheng Zhang
Liangjun Lu
Jianping Chen

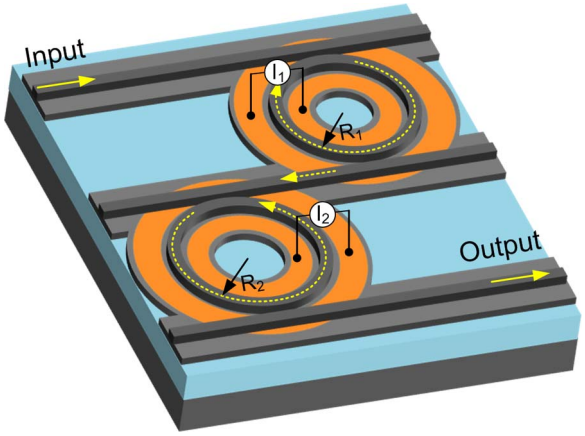

DOI: 10.1109/JPHOT.2013.2271901
1943-0655/$31.00 ©2013 IEEE

IEEE photonics SOCIETY

IEEE

Tunable Vernier Microring Optical Filters With $p-i-p$-Type Microheaters

Linjie Zhou, *Member, IEEE*, Xiaoheng Zhang, Liangjun Lu, and Jianping Chen

State Key Laboratory of Advanced Optical Communication Systems and Networks, Department of Electronic Engineering, Shanghai Jiao Tong University, Shanghai 200240, China

DOI: 10.1109/JPHOT.2013.2271901
1943-0655/$31.00 ©2013 IEEE

Manuscript received May 29, 2013; revised June 26, 2013; accepted June 27, 2013. Date of publication July 3, 2013; date of current version July 10, 2013. This work was supported in part by the 973 Program under Grant ID2011CB301700; by the 863 Program under Grant 2013AA014402; by the National Natural Science Foundation of China (NSFC) under Grants 61007039, 61001074, and 61127016; by the Science and Technology Commission of Shanghai Municipality (STCSM) under Projects 10DJ1400402 and 12XD1406400; and by the State Key Laboratory Project under Grant GKZD030024. Corresponding author: L. Zhou (e-mail: ljzhou@sjtu.edu.cn).

Abstract: We present thermally tunable microring optical filters using $p-i-p$-type microheaters. The use of Vernier effect in the cascaded two microring resonators significantly enlarges the free spectral range (FSR) and the thermal tuning range with reduced power consumption. Heat generated by the $p-i-p$-type microheaters interacts directly with the microring waveguides, providing a means to effectively tune resonances without incurring excess loss. Experimental results reveal that the filter passband can be discretely shifted in the wavelength range from 1520 to 1600 nm by tuning one resonator with a power tuning efficiency value of 2.5 nm/mW. The passband can be also continuously shifted by simultaneously tuning both resonators with a power tuning efficiency value of 0.11 nm/mW. The rise (fall) time of the $p-i-p$ microheater is measured to be 460 ns (1.1 μs) under a peak-to-peak driving voltage of 3.4 V.

Index Terms: Wavelength filter, microring resonator, thermo-optic devices, silicon photonics, integrated optics devices.

1. Introduction

Optical filters are one of the essential key components in multichannel optical signal processing applications. In wavelength division multiplexing (WDM) based telecom and datacom routing [1], [2], wavelengths need to be extracted using optical filters from a bank of WDM channels for local processing. Optical filters can also be employed in RF-photonic processing and analog photonic link to provide ultra-broad bandwidth, agile complex functionality, and potentially low power consumption, which otherwise could not be achieved by using the traditional electrical signal processing approaches [3], [4].

Optical filters can be categorized into infinite impulse response (IIR) and finite impulse response (FIR) with the former usually incorporating resonance feedback and the latter only feed-forward interference [5]. A variety of structures can be employed to form integrated optical filters, such as Mach–Zehnder interferometers (MZIs) [6]–[9], Bragg gratings [10]–[13], Fabry–Perot resonators [14], [15], microring/microdisk resonators [16]–[24], and more sophisticated MZI-ring combined structures [25]–[28]. Micro-resonator based optical filters on silicon-on-insulator (SOI) material platform have the advantages of compact size, high finesse, and versatility.

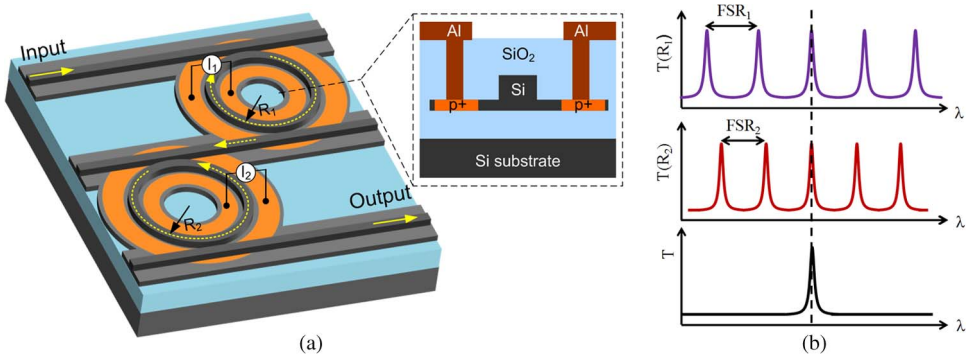

Fig. 1. (a) Schematic illustration of the tunable Vernier microring optical filter. Inset shows the cross section of the microring resonators. (b) Vernier operation principle using two microring resonators.

Multichannel WDM systems require an optical filter to select a single wavelength channel in a broad spectral range. For micro-resonator based optical filters, this means the spacing between adjacent resonance peaks or the free spectral range (FSR) should be large. A large FSR helps to improve the multiplexing of a great number of channels. As FSR is inversely proportional to the resonator size, a small resonator has to be chosen in order to get a large FSR [29], [30]. Reducing resonator dimension inevitably results in a higher loss, which in turn sacrifices the resonance Q-factor or the filter selectivity. Another way to increase FSR is to use a pulley or U-shaped waveguide to couple with the resonator [31], [32]. Grating can also be incorporated into the coupling region for selective excitation of resonances [33]. In these structures, the phase match condition in coupling is fully utilized. However, it is quite challenging in device design and fabrication to suppress the adjacent resonances to a negligible level. Directly-coupled or sequentially-coupled microring resonators with slightly different radii give rise to Vernier effect, which can effectively expand the filtering channel FSR [34], [35].

Owing to its resonance nature, the central wavelength of microring filters is very sensitive to design parameters and fabrication conditions, and thus it is hard to accurately predict their filter wavelength. Active tuning is a viable solution to address this issue, which is also a desirable feature in applications requiring wavelength tunability to listen to different channels [36]. There are two commonly used effects in silicon to tune the refractive index, namely, the thermo-optic effect and the free-carrier plasma dispersion effect [37]. The former one is a slow yet relatively strong effect, which can result in a large refractive index change with no excess loss. The latter one, on the other hand, is a fast and yet its refractive index change is limited by the free-carrier absorption loss. In order to get a large tuning range desired in a tunable filter, thermal approach is usually a preferred option. However, thermal power consumption is relatively high to shift one FSR. Using Vernier effect is an effective way to reduce the power consumption while getting a large tuning range.

In this paper, we report a thermally tunable optical filter based on two sequentially connected microring resonators making use of the Vernier effect [38]. The tuning is enabled via the integrated $p-i-p$ micro-heaters. The microrings can be tuned either individually or simultaneously, resulting in discrete or continuous shift of the filter passband, respectively. Owing to the direct interaction between generated heat and waveguide mode, the thermal tuning has a relatively fast response.

2. Working Principle and Simulation

Fig. 1(a) shows the 3-D perspective view of the Vernier microring optical filter. It consists of two microring resonators coupled with three parallel waveguides. The two microrings have slightly different bending radii, so that only when the input light is resonant with both microrings can the light be transmitted to the output port. To tune the microring resonators, we embed $p-i-p$ type micro-heaters into each microring waveguide as shown by the inset of Fig. 1(a). When current flows through the $p-i-p$ micro-heater, heat will be generated, leading to a refractive index change of

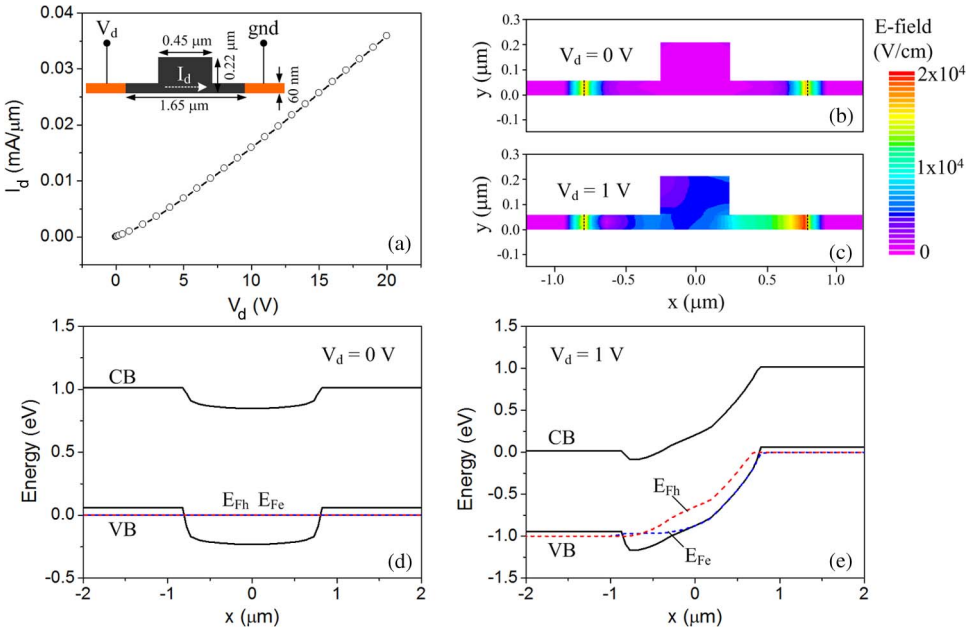

Fig. 2. (a) 2-D simulated *I–V* curve of the $p-i-p$ micro-heater. (b) Electric field distribution at 0 V. (c) Electric field distribution at 1 V. (d) Energy band diagram at 0 V. (e) Energy band diagram at 1 V.

the waveguide due to the thermo-optic effect of silicon. Fig. 1(b) illustrates the working mechanism of the microring Vernier tuning. The larger microring has a smaller FSR. When the resonances from the two microrings are aligned, there appears a common resonance peak. Otherwise, no resonance shows up at the output port. The common FSR of the Vernier filter is $FSR_c = mFSR_1 = nFSR_2$ (m and n are integers). The closer FSR_1 and FSR_2 are, the larger FSR_c is. We can tune one microring to shift its resonance a little bit to align the next set of resonances, and then the Vernier resonance experiences a large shift (FSR_1 or FSR_2). In this way, the Vernier filter is discretely tuned. If both microrings are tuned simultaneously, then the Vernier resonance can be set to any wavelength. In this case, we get continuous tuning of the Vernier filter.

In our tunable filter design, we make full use of the *p*-type doping to devise a micro-heater which is directly integrated with the microring waveguide. Because the heater is based on $p-i-p$ semiconductor junctions, its behavior is distinct from a pure metal resistor-based heater. In order to investigate its electrical characteristics, we employed a 2-D simulation package, ATLAS from SILVACO for the numerical calculation. The software simulates the electrical characteristics of semiconductor devices by solving the Poisson's and charge continuity equations for electrons and holes. In our simulation, the device parameters are the same with our real device. The waveguide width is 0.45 μm and the height is 220 nm with a 60 nm slab remained for the lateral $p-i-p$ structure. The highly *p*-type doped regions have a doping concentration of 10^{20} cm^{-3}. The highly-doped regions are separated from the waveguide by 0.6 μm to ensure low free carrier absorption loss. It should be noted that the waveguide is not exactly intrinsic but is lightly *p*-type doped with a concentration of 10^{15} cm^{-3}. The electron and hole carrier life times are assumed to be 100 ns. Ohmic contacts with no additional resistance or capacitance are used for the two electrodes.

Fig. 2(a) shows the simulated current-voltage (*I–V*) curve. The resistance is around 560 k$\Omega \cdot \mu$m. Fig. 2(b) and (c) depict the electric field distribution in the cross section for 0 V and 1 V, respectively. Due to the difference in doping concentration, holes diffuse from the high concentration to the low concentration regions until it is balanced by the reverse drift current. Electric field eventually builds up at the $p-i$ and $i-p$ junctions. Without an external voltage, the electric field distribution is symmetric at the two junctions. However, after applying a positive voltage at the left terminal, the symmetry is broken, leading to higher electric field at the right $i-p$ junction. To more clearly

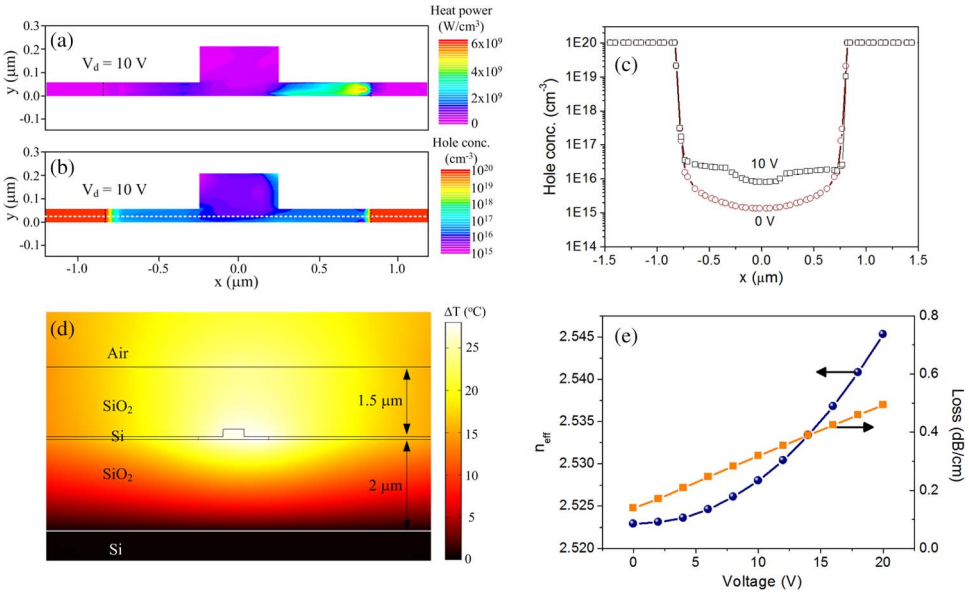

Fig. 3. (a) Heat power density and (b) hole concentration distributions in the $p-i-p$ micro-heater at 10 V. (c) Comparison of the hole concentration distribution along the slab region of the waveguide at 0 V and 10 V. (d) Temperature rise of the silicon waveguide at 10 V. (e) Waveguide effective refractive index and excess propagation loss change with the driving voltage.

interpret the electrical behavior of the $p-i-p$ junctions, we plot the energy band diagram at 0 V and 1 V in Fig. 2(d) and (e), respectively. At 0 V, the junctions are at equilibrium with the electron and hole quasi-Fermi levels being an overlapped straight horizontal line. Both valance and conduction bands drop from the high doping concentration region to the quasi-intrinsic region at the two junctions, where the built-in electric field is formed. When a positive external voltage is applied to the left terminal, the band at the right side is leveled up. The external voltage is largely dropped at the right $i-p$ junction while the initial barrier height at the left $p-i$ junction is a little lowered. It seems that the left junction is forward-biased and the right reverse-biased. The quasi-Fermi levels become split and crossed in the quasi-intrinsic region. As the barrier height is reduced at the left junction, holes are diffused into the quasi-intrinsic region and then swept to the other terminal by the electric field which is particularly strong close to the right junction as seen from Fig. 2(c). Therefore, the total current (primarily the hole current) is determined by the $p-i$ junction barrier height. In regard of this, its I–V characteristic is in principle distinct from that of a pure resistor.

Current flows though the $p-i-p$ structure to generate heat power P, which is given by $P = \boldsymbol{J} \cdot \boldsymbol{E}$, where $\boldsymbol{J}$ is the current density and $\boldsymbol{E}$ is the electric field. Because electric field is high around the $i-p$ junction, heat is mainly generated there. Fig. 3(a) shows the heat power density contour in the waveguide cross section at 10 V. As expected, heat power density is much higher at the right junction than at the left junction. With the increase in applied voltage, the injected hole concentration in the quasi-intrinsic region is also increased as shown in Fig. 3(b). Fig. 3(c) shows the hole concentration distribution along the horizontal line in the slab for both 0 V and 10 V. It reveals that the hole concentration in the waveguide region increases from the original 10^{15} cm^{-3} to 10^{16} cm^{-3} after the $p-i-p$ micro-heater is turned on. To simulate the influence of heat power on the waveguide effective refractive index, we employed the commercial finite element method (FEM) package (COMSOL). The thermo-optic coefficients of silicon and silica are chosen to be 1.86×10^{-4} k^{-1} and 1.0×10^{-5} k^{-1}, respectively. Fig. 3(d) shows the temperature rise of the waveguide. Although the heat power density peak is not exactly overlapped with the waveguide core, the generated heat can diffuse and interact with the waveguide core to raise its temperature without significant temperature gradient across the waveguide. The waveguide temperature rises

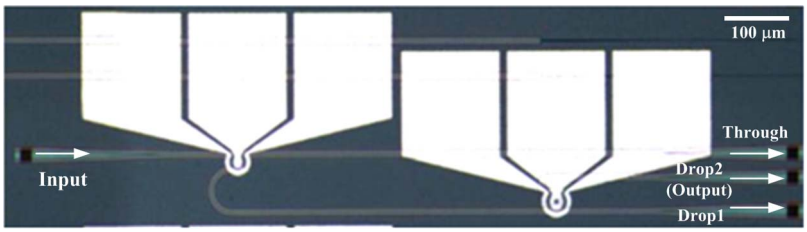

Fig. 4. Microscope image of the fabricated tunable Vernier microring optical filter.

by 27 °C at 10 V driving voltage (0.16 mW/μm heat power). The waveguide effective refractive index is affected by both the temperature rise and the free-carrier concentration increase. Fig. 3(e) shows the simulated waveguide effective refractive index and propagation loss change with the driving voltage. The parabolic curve of n_{eff} originates from the quadratic dependence of heat power on driving voltage. The waveguide propagation loss increases linearly with voltage. The free carrier absorption induced excess loss is less than 0.5 dB/cm even at a very high voltage of 20 V (corresponding to 0.72 mW/μm heat power). We will show in our experiment that such heat power is enough to tune the Vernier filter across 10's nm spectral range.

It should be noted that the $p-i-p$ type micro-heater is structurally very similar to the conventional $p-i-n$ diode routinely used for silicon refractive index tuning based on the free-carrier plasma dispersion effect. Therefore, the fabrication of $p-i-p$ micro-heaters is totally compatible with $p-i-n$ diodes with no addition fabrication steps. The underlying physics of $p-i-p$ structure is much richer than one might think of at the first glance. We believe such fundamental understanding is useful in $p-i-p$ micro-heater design for thermally tunable silicon photonic devices.

3. Device Fabrication and Experimental Results

Based on the above principle, we designed and fabricated a tunable Vernier filter composed of two microrings with slightly different radii of $R_1 = 10$ μm and $R_2 = 11$ μm. The fabrication begins with a silicon-on-insulator (SOI) wafer. The top silicon layer is 220 nm thick and the bottom buried oxide layer is 2 μm thick. Deep ultra-violet (DUV) photolithography using a 248 nm stepper was employed to define the waveguide patterns, followed by anisotropic dry etch of silicon. Boron ion implantation was performed to form the highly *p*-type doped regions. The slab layer was also etched outside the $p-i-p$ junctions so as to reduce heat diffusion through the slab. Finally, contact holes were etched and aluminum was deposited to form the metal connection. The whole fabrication process is done in IME Singapore using complementary metal-oxide-semiconductor (CMOS) compatible processes. Fig. 4 shows the microscope image of the fabricated device. The input port is at the left side and the three output ports (through, drop1, and drop2) are routed to the right side. The drop2 port is the Vernier output port. The gap between the ring and the bus waveguide is 200 nm. To couple light in and out of the waveguides, grating couplers with a 630 nm period and a 70 nm shallow etch depth are used.

Fig. 5(a) shows the measured transmission spectra of the through and output ports for transverse electric (TE) polarization. As grating couplers are used for input and output coupling, there is a transmission envelope centered at 1550 nm in the spectra. The fiber-to-fiber insertion loss for the through port is around 20 dB at the grating central wavelength. The silicon waveguide propagation loss is 3–4 dB/cm measured from test waveguides. The high insertion loss is mainly due to the fiber-waveguide coupling loss, which can be improved by using optimized grating couplers [39]. The through port spectrum is generated by only the first microring, and therefore, it exhibits uniformly-spaced resonance dips with a FSR of 9.5 nm around 1550 nm. The resonance Q-factor is 9×10^3 (linewidth $\sim$0.17 nm) and the extinction ratio (ER) is $\sim$20 dB. The as-fabricated two microring resonators do not have their resonances well aligned, leading to two small resonance peeks

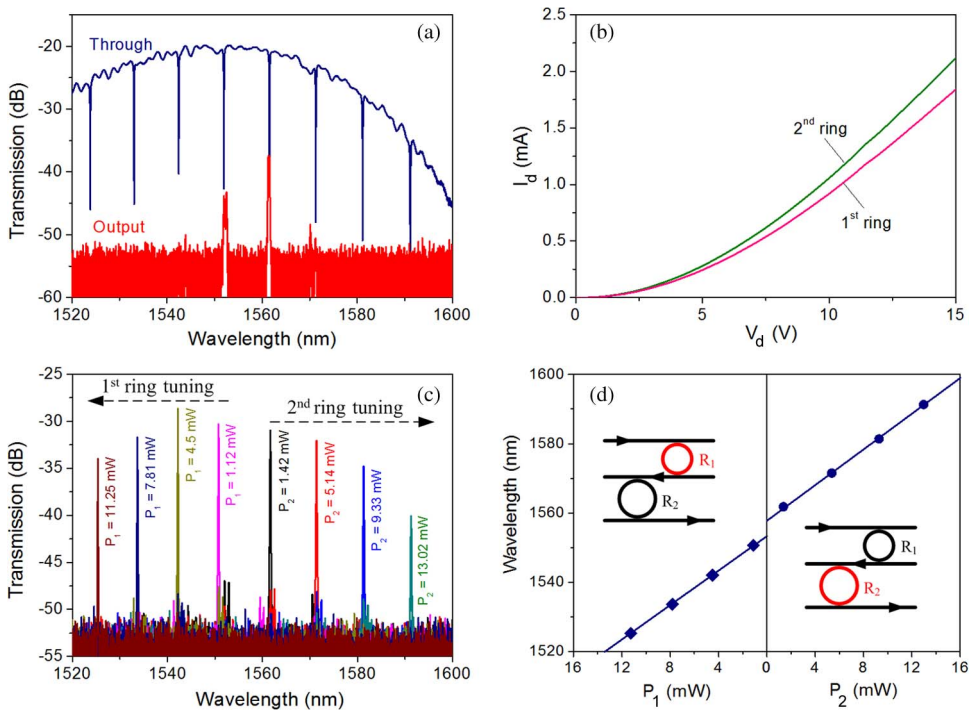

Fig. 5. (a) Transmission spectra of the Vernier microring filter without active tuning. (b) Measured *I*–*V* curves of the two microring resonators. (c) Vernier tuning of the output spectrum. Either the 1st or the 2nd microring resonator is tuned. (d) Extracted filter central wavelength as a function of tuning power.

observable in the output port. To generate a single Vernier resonance, either the 1st or the 2nd microring should be carefully tuned.

To actively tune the resonators, we used metal probes to connect the electrodes of the $p-i-p$ micro-heater to external current sources. Voltmeters were used to monitor the voltage on the $p-i-p$ micro-heater, and hence the power consumption can be calculated. Fig. 5(b) shows the measured *I*–*V* curves for the two microring resonators. The resistance is in the order of 10 kΩ. Fig. 5(c) illustrates the Vernier resonance shift upon tuning of the 1st (tuning power P_1) or the 2nd (tuning power P_2) microring. Only one pronounced Vernier resonance peak is observable from 1520 to 1600 nm after the two microrings are well aligned. When tuning is performed to the 1st microring, the Vernier resonance is shifted to the short wavelength side with a discrete step size of 8.6 nm, which is corresponding to the FSR of the 2nd microring resonator. It is expected since the 1st microring has a larger FSR due to its smaller size and the thermo-optic effect will induce a red shift, and therefore the overall effect is that their common resonance experiences a blue-jump with a step size corresponding to FSR_2. On the contrary, when tuning is performed to the 2nd microring, the Vernier resonance experiences a discrete red-shift with a step size of FSR_1 instead. The extended Vernier FSR is ∼95 nm by estimation (not shown in the measured spectral range), which is 10 and 11 times larger than that of the 1st and 2nd microring resonators, respectively. In the Vernier output, the interstitial peak suppression (the difference between the major peak and the highest side peak) is around 16 dB, as can be seen from Fig. 5(c). The additional loss for the Vernier output port is ∼8 dB. The Vernier resonance peaks follow the envelope of the grating coupler spectrum. If other broadband coupler structures like the inverse tapers [40] are used, the Vernier peak powers could be better equalized.

We extract the Vernier resonance wavelength and plot it as a function of tuning power shown in Fig. 5(d). Both tunings follow a straight line with almost the same tuning efficiency of 2.5 nm/mW. To move one Vernier step, the tuning microring has to shift a fixed value of $\Delta\lambda_r = |FSR_1 - FSR_2|$ no matter which one is actively tuned. However, the Vernier step is determined by the other microring

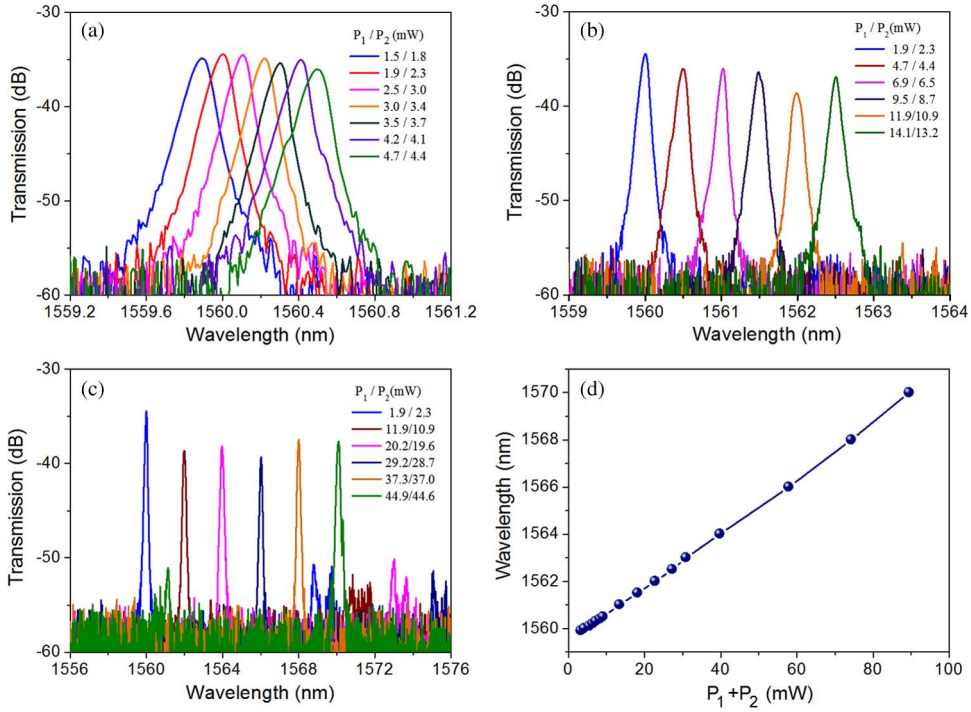

Fig. 6. (a)-(c) Output spectrum tuning with a step of (a) 0.1 nm, (b) 0.5 nm, and (c) 1.0 nm. The two microring resonators are tuned simultaneously. (d) Extracted filter central wavelength as a function of total tuning power consumption.

resonator, i.e., $\Delta\lambda_{v1} = FSR_2$ and $\Delta\lambda_{v2} = FSR_1$. The tuning efficiency is given by $\eta_i = \Delta\lambda_{vi}/\Delta P_{ri}$ ($i = 1, 2$ for tuning of the 1st and the 2nd microrings, respectively), where ΔP_{ri} is the tuning power associated with resonance shift $\Delta\lambda_r$. From the resonance condition, we know that the resonance wavelength shift is proportional to the microring waveguide effective refractive index change, i.e., $\Delta\lambda_r/\lambda = \Delta n_{eff}/n_{eff}$. On the other hand, the effective index change is proportional to the tuning power per unit length, i.e., $\Delta n_{eff} = a\Delta P_{ri}/(2\pi R_i)$, where a is a constant coefficient determined by the $p - i - p$ micro-heater. Therefore, we have

$$\eta_{1,2} = \frac{a\lambda FSR_{2,1}}{(2\pi R_{1,2}) n_{eff}(FSR_1 - FSR_2)} = \frac{a\lambda}{2\pi(R_2 - R_1) n_{eff}}. \quad (1)$$

In deriving the above equation, we expanded the FSR as $FSR_i = \lambda^2/(2\pi R_i n_g)$where n_g is the microring waveguide group refractive index. It can be seen from Eq. (1) that the tuning efficiency is microring independent. In order to get a high tuning efficiency, either a highly efficient micro-heater should be used or the size of the two microrings should be very close. However, because of the Lorentzian line shape of resonances, reducing the size difference will generate side Vernier peaks, degrading the purity of the output spectrum.

Other than tuning one microring resonator to get a discrete shift of the Vernier resonance, the two microrings can be tuned simultaneously, and in this case a continuous shift of the resonance can be obtained. Fig. 6(a) shows the red shift of the Vernier output resonance when both microrings are carefully tuned to achieve a step shift of 0.1 nm. The ER is kept at 20 dB. With an increased tuning power in both microrings, a larger continuous shift range can be obtained as shown in Fig. 6(b) and (c). The shift step is set at 0.5 and 2 nm, respectively. With a total power consumption of 90 mW, the resonance is red shifted by 10.1 nm, exceeding one FSR of the individual microring resonators. Hence, it demonstrates that the filter can be coarsely tuned to cover a large spectral range thanks to the Vernier effect, while it still can be finely tuned within one FSR by heating both resonators. Fig. 6(d)

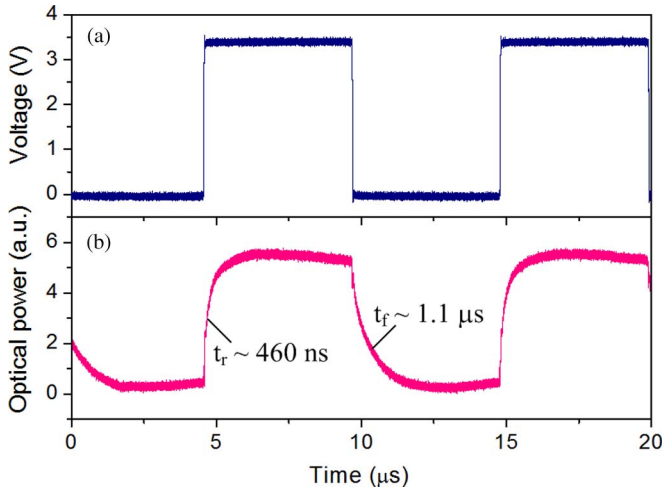

Fig. 7. Time-domain response of the 1st microring resonator as a switch. (a) Applied electrical waveform; (b) Measured optical waveform at the through port.

shows the extracted filter central wavelength changes as a function of total power consumption on the microring resonators. From linear fitting, we obtain the power tuning efficiency of 0.11 nm/mW.

We also characterized the tuning speed of the Vernier filter by measuring the time-domain response of the microring resonator. An electrical square-wave signal is applied to the 1st microring resonator so that its resonance is modulated by the electrical signal, leading to a square-wave optical signal at the through port. Fig. 7(a) and (b) show the electrical and modulated optical waveforms measured using an oscilloscope. A 5 GHz bandwidth receiver is used in recording the optical waveform. The optical wavelength is set at the resonance wavelength, and thereby the resulting optical waveform follows the electrical counterpart. The on-cycle voltage of the electrical signal is 3.4 V, corresponding to 0.38 mW heating power. The rise time of the optical waveform, defined as 10% to 90% of the optical power, is measured to be 460 ns. The corresponding fall time is 1.1 μs, longer than the rise time. It suggests that the microring resonator is easier to be heated up than cooled down, since heat is generated through direct resistive heating of the waveguide during on-cycle and yet it has to diffuse away to cool down the waveguide during the off-cycle.

4. Discussions

For thermal tuning of silicon photonic devices, metal heaters are widely used where high resistivity metal (W, Ti, TiN etc.) is positioned on top of the silicon waveguide. Because metal has high absorption loss, it cannot be put very close to the waveguide. Usually 1-2 micron oxide layer is overclad on the waveguide to separate them. Therefore, such structural arrangement makes the metal heater not efficient in terms of power tuning efficiency and temporal response. Heat has to diffuse through the top low thermal-conductivity oxide layer to interact with the waveguide. The reported tuning power ranges from 35 to 105 mW per 2π-phase shift (equivalent to one FSR shift in microring resonators) without using thermal isolation [41]. For our $p-i-p$ type micro-heater, we can deduce the thermal tuning efficiency for each microring from Fig. 6(c). To continuously shift 10.1 nm, the power consumption of the 1st and 2nd microring resonators are 43 and 42.3 mW, respectively. The thermal tuning power per FSR is thus 40 and 36 mW for the two individual resonators. Therefore, our $p-i-p$ type micro-heater is at the lower end compared to metal heaters. The response time of metal heaters is usually a few μs [42]. Our device has a response time of 460 ns and 1.1 μs, several times lower than that of metal heaters. It is expected since our $p-i-p$ type micro-heater directly heats up the waveguide without thermal diffusion.

Another type of micro-heaters is based on silicon resistor formed by *n*-type or *p*-type doping. For example, Watts *et al.* reported a micro-heater integrated directly on an adiabatic silicon waveguide

with n-type doping concentration of 1.8×10^{18} cm^{-3} [43]. The thermal power is $\sim$25.4 mW/2π-phase shift, lower than our structure. Their response time is 2.4 μs, longer than ours. In principle, the tuning efficiency and power consumption of both structures should be similar because they all use silicon as the heat source. In our structure, the contact holes (infiltrated with metal) are only 1.6 μm away from the silicon waveguide edge [see Fig. 1(a) inset]. As metal is a very good thermal conductor, such design increases the power consumption and meanwhile it speeds up the temporal response. In fact, there is a tradeoff between the power consumption and the response time. If we put metal contact far from the waveguide and use air trenches to isolate the $p-i-p$ micro-heater, then it is possible to reduce the tuning power consumption at the expense of lowered response speed. It should be noted that the filter wavelength tuning efficiency is greatly improved by using the Vernier effect. In our device, the Vernier tuning mode is $\sim$23 times more efficient that the continuous tuning mode. The voltage drop in our $p-i-p$ micro-heater is still high because of the low doping $(10^{15}$ cm$^{-3})$ in the silicon waveguide region. If its doping concentration is leveled up to 10^{17} cm^{-3} (excess loss $<$ 2 dB/cm), then the voltage can be reduced by 3–5 times according to our simulation.

5. Conclusion

We demonstrated thermally tunable Vernier microring optical filters. Thermal tuning is enabled by using $p-i-p$ type micro-heaters integrated directly in microring waveguides. Numerical simulations revealed that $p-i-p$ type structure resembles but is not exactly the same as a pure resistor in that it exhibits junction-like features. Heat is generated asymmetrically from the junction close to the lower potential end. Free carrier induced waveguide loss slightly increases with heat power, but is still within an acceptable level of $<$ 0.5 dB/cm even at 20 V. Experiments demonstrated that the Vernier microring filter output only exhibits a single passband in the wavelength range from 1520 nm to 1600 nm. Two tuning approaches were used to shift the filter passband. In the first one, the microrings were tuned independently and owing to the Vernier effect, the passband can be red- or blue-shifted with a step size corresponding to the microring FSRs. The tuning efficiency is 2.5 nm/mW. In the second one, the microrings were tuned simultaneously so that the desired resonances from the two microrings were always aligned, leading to continuous shift of the filter passband. The tuning efficiency is 0.11 nm/mW. The former approach works as a coarse tuning knob and the latter as a fine knob. By combining these two approaches, the filter passband can be tuned to cover one common FSR of $\sim$95 nm with power consumption much lower than that of a regular microring filter without Vernier effect. We also characterized the temporal response of the $p-i-p$ type micro-heater. The measured rise time and fall time in response to a 3.4 V square wave electrical signal are 460 ns and 1.1 μs, respectively. Such long-range tunable optical filters are potentially useful in WDM optical links for telecom and datacom applications.

Acknowledgment

The authors acknowledge IME Singapore for device fabrication.

References

[1] A. Benner, D. M. Kuchta, P. K. Pepeljugoski, R. A. Budd, G. Hougham, B. V. Fasano, K. Marston, H. Bagheri, E. J. Seminaro, H. Xu, D. Meadowcroft, M. H. Fields, L. McColloch, M. Robinson, F. W. Miller, R. Kaneshiro, R. Granger, D. Childers, and E. Childers, "Optics for high-performance servers and supercomputers," presented at the Proc. Opt. Fiber Commun. Conf., San Diego, CA, USA, 2010, OTuH.

[2] A. Nag, M. Tornatore, and B. Mukherjee, "Optical network design with mixed line rates and multiple modulation formats," *J. Lightw. Technol.*, vol. 28, no. 4, pp. 466–475, Feb. 2010.

[3] R. A. Minasian, "Photonic signal processing of microwave signals," *IEEE Trans. Microw. Theory Tech.*, vol. 54, no. 2, pp. 832–846, Feb. 2006.

[4] V. J. Urick, F. Bucholtz, J. D. McKinney, P. S. Devgan, A. L. Campillo, J. L. Dexter, and K. J. Williams, "Long-haul analog photonics," *J. Lightw. Technol.*, vol. 29, no. 8, pp. 1182–1205, Apr. 2011.

[5] C. K. Madsen and J. H. Zhao, *Optical Filter Design and Analysis: A Signal Processing Approach*. Hoboken, NJ, USA: Wiley, 2001.

[6] L. Lu, L. Zhou, X. Sun, J. Xie, Z. Zou, H. Zhu, X. Li, and J. Chen, "CMOS-compatible temperature-independent tunable silicon optical lattice filters," *Opt. Exp.*, vol. 21, no. 8, pp. 9447–9456, Apr. 2013.

[7] H. Yu, M. Chen, P. Li, S. Yang, H. Chen, and S. Xie, "Silicon-on-insulator narrow-passband filter based on cascaded MZIs incorporating enhanced FSR for downconverting analog photonic links," *Opt. Exp.*, vol. 21, no. 6, pp. 6749–6755, Mar. 2013.
[8] F. Horst, W. M. Green, S. Assefa, S. M. Shank, Y. A. Vlasov, and B. J. Offrein, "Cascaded Mach–Zehnder wavelength filters in silicon photonics for low loss and flat pass-band WDM (de-) multiplexing," *Opt. Exp.*, vol. 21, no. 10, pp. 11 652–11 658, May 2013.
[9] K. Yamada, T. Shoji, T. Tsuchizawa, T. Watanabe, J.-i. Takahashi, and S.-i. Itabashi, "Silicon-wire-based ultrasmall lattice filters with wide free spectral ranges," *Opt. Lett.*, vol. 28, no. 18, pp. 1663–1664, Sep. 2003.
[10] Y. Painchaud, M. Poulin, C. Latrasse, N. Ayotte, M.-J. Picard, and M. Morin, "Bragg grating notch filters in silicon-on-insulator waveguides," presented at the Proc. Bragg Gratings, Photosens., Poling Glass Waveguides, Colorado Springs, CO, USA, 2012, BW2E.
[11] H. Qiu, G. Jiang, T. Hu, H. Shao, P. Yu, J. Yang, and X. Jiang, "FSR-free add-drop filter based on silicon grating-assisted contradirectional couplers," *Opt. Lett.*, vol. 38, no. 1, pp. 1–3, Jan. 2013.
[12] G. Jiang, R. Chen, Q. Zhou, J. Yang, M. Wang, and X. Jiang, "Slab-modulated sidewall Bragg gratings in silicon-on-insulator ridge waveguides," *IEEE Photon. Technol. Lett.*, vol. 23, no. 1, pp. 6–8, Jan. 2011.
[13] Z. Zhang, D. Liu, D. de Felipe, A. Liu, N. Keil, and N. Grote, "Polymer embedded silicon nitride thermally tunable Bragg grating filters," *Appl. Phys. Lett.*, vol. 102, no. 18, pp. 181105-1–181105-4, May 2013.
[14] X. Sun, L. Zhou, J. Xie, Z. Zou, L. Lu, X. Li, and J. Chen, "Tunable silicon comb filters based on Fabry–Perot resonators formed by Sagnac loop mirrors," *Opt. Lett.*, vol. 38, no. 4, pp. 567–569, Feb. 2013.
[15] M. Ménard and A. G. Kirk, "Integrated Fabry–Perot comb filters for optical space switching," *J. Lightw. Technol.*, vol. 28, no. 5, pp. 768–775, Mar. 2010.
[16] L. Zhou and A. W. Poon, "Electrically reconfigurable silicon microring resonator-based filter with waveguide-coupled feedback," *Opt. Exp.*, vol. 15, no. 15, pp. 9194–9204, Jul. 2007.
[17] P. Dong, N.-N. Feng, D. Feng, W. Qian, H. Liang, D. C. Lee, B. J. Luff, T. Banwell, A. Agarwal, P. Toliver, R. Menendez, T. K. Woodward, and M. Asghari, "GHz-bandwidth optical filters based on high-order silicon ring resonators," *Opt. Exp.*, vol. 18, no. 23, pp. 23 784–23 789, Nov. 2010.
[18] J. E. Cunningham, I. Shubin, X. Zheng, T. Pinguet, A. Mekis, Y. Luo, H. Thacker, G. Li, J. Yao, K. Raj, and A. V. Krishnamoorthy, "Highly-efficient thermally-tuned resonant optical filters," *Opt. Exp.*, vol. 18, no. 18, pp. 19 055–19 063, Aug. 2010.
[19] C. Li, J. H. Song, J. Zhang, H. Zhang, S. Chen, and M. Yu, "Silicon polarization independent microring resonator-based optical tunable filter circuit with fiber assembly," *Opt. Exp.*, vol. 19, no. 16, pp. 15 429–15 437, Aug. 2011.
[20] M. Geng, L. Jia, L. Zhang, L. Yang, P. Chen, T. Wang, and Y. Liu, "Four-channel reconfigurable optical add-drop multiplexer based on photonic wire waveguide," *Opt. Exp.*, vol. 17, no. 7, pp. 5502–5516, Mar. 2009.
[21] Q. Huang, X. Zhang, J. Xia, and J. Yu, "Dual-band optical filter based on a single microdisk resonator," *Opt. Lett.*, vol. 36, no. 23, pp. 4494–4496, Dec. 2011.
[22] Q. Li, A. A. Eftekhar, P. Alipour, A. H. Atabaki, S. Yegnanarayanan, and A. Adibi, "Low-loss microdisk-based delay lines for narrowband optical filters," *IEEE Photon. Technol. Lett.*, vol. 24, no. 15, pp. 1276–1278, Aug. 2012.
[23] T. Barwicz, P. Rakich, M. Watts, H. Haus, E. Ippen, and H. Smith, "Microring-resonator-based add-drop filters in SiN: Fabrication and analysis," *Opt. Exp.*, vol. 12, no. 7, pp. 1437–1442, Apr. 2004.
[24] S. J. Emelett and R. Soref, "Design and simulation of silicon microring optical routing switches," *J. Lightw. Technol.*, vol. 23, no. 4, pp. 1800–1807, Apr. 2005.
[25] S. Djordjevic, L. Luo, S. Ibrahim, N. Fontaine, C. Poitras, B. Guan, L. Zhou, K. Okamoto, Z. Ding, M. Lipson, and S. J. B. Yoo, "Fully reconfigurable silicon photonic lattice filters with four cascaded unit cells," *IEEE Photon. Technol. Lett.*, vol. 23, no. 1, pp. 42–44, Jan. 2011.
[26] N.-N. Feng, P. Dong, D. Feng, W. Qian, H. Liang, D. C. Lee, J. B. Luff, A. Agarwal, T. Banwell, R. Menendez, P. Toliver, T. K. Woodward, and M. Asghari, "Thermally-efficient reconfigurable narrowband RF-photonic filter," *Opt. Exp.*, vol. 18, no. 24, pp. 24 648–24 653, Nov. 2010.
[27] L. Zhou, T. Ye, and J. Chen, "Waveguide self-coupling based reconfigurable resonance structure for optical filtering and delay," *Opt. Exp.*, vol. 19, no. 9, pp. 8032–8044, Apr. 2011.
[28] L. Zhou and A. W. Poon, "Fano resonance-based electrically reconfigurable add-drop filters in silicon microring resonator-coupled Mach–Zehnder interferometers," *Opt. Lett.*, vol. 32, no. 7, pp. 781–783, Apr. 2007.
[29] M. S. Nawrocka, T. Liu, X. Wang, and R. R. Panepucci, "Tunable silicon microring resonator with wide free spectral range," *Appl. Phys. Lett.*, vol. 89, no. 7, pp. 071110-1–071110-3, Aug. 2006.
[30] Q. Xu, D. Fattal, and R. G. Beausoleil, "Silicon microring resonators with 1.5-μm radius," *Opt. Exp.*, vol. 16, no. 6, pp. 4309–4315, Mar. 2008.
[31] J. Xie, L. Zhou, Z. Zou, L. Lu, H. Zhu, X. Sun, X. Li, and J. Chen, "Selective excitation of microring resonances using a pulley-coupling structure," presented at the Proc. 10th Conf. Lasers Electro-Opt. Pac. Rim, Proc. 18th OptoElectron. Commun. Conf./Photon. Switching, Kyoto, Japan, 2013, WL4-3.
[32] E. S. Hosseini, S. Yegnanarayanan, A. H. Atabaki, M. Soltani, and A. Adibi, "Systematic design and fabrication of high-Q single-mode pulley-coupled planar silicon nitride microdisk resonators at visible wavelengths," *Opt. Exp.*, vol. 18, no. 3, pp. 2127–2136, Feb. 2010.
[33] W. Shi, X. Wang, W. Zhang, H. Yun, C. Lin, L. Chrostowski, and N. A. F. Jaeger, "Grating-coupled silicon microring resonators," *Appl. Phys. Lett.*, vol. 100, no. 12, pp. 121118-1–121118-4, Mar. 2012.
[34] R. Boeck, N. A. Jaeger, N. Rouger, and L. Chrostowski, "Series-coupled silicon racetrack resonators and the Vernier effect: Theory and measurement," *Opt. Exp.*, vol. 18, no. 24, pp. 25 151–25 157, Nov. 2010.
[35] R. Boeck, J. Flueckiger, H. Yun, L. Chrostowski, and N. A. Jaeger, "High performance Vernier racetrack resonators," *Opt. Lett.*, vol. 37, no. 24, pp. 5199–5201, Dec. 2012.
[36] A. V. Krishnamoorthy, R. Ho, X. Zheng, H. Schwetman, J. Lexau, P. Koka, G. Li, I. Shubin, and J. E. Cunningham, "Computer systems based on silicon photonic interconnects," *Proc. IEEE*, vol. 97, no. 7, pp. 1337–1361, Jul. 2009.
[37] G. T. Reed and A. P. Knights, *Silicon Photonics*. Hoboken, NJ, USA: Wiley, 2008.

[38] X. Zhang, L. Zhou, L. Lu, J. Xie, X. Sun, X. Li, and J. Chen, "Tunable Vernier microring optical filters using p-i-p resistor-based micro-heaters," presented at the Proc. OFC, Anaheim, CA, USA, 2013, OTu3C.
[39] A. Mekis, S. Gloeckner, G. Masini, A. Narasimha, T. Pinguet, S. Sahni, and P. De Dobbelaere, "A grating-coupler-enabled CMOS photonics platform," *IEEE J. Sel. Topics Quantum Electron.*, vol. 17, no. 3, pp. 597–608, May/Jun. 2011.
[40] T. Shoji, T. Tsuchizawa, T. Watanabe, K. Yamada, and H. Morita, "Low loss mode size converter from 0.3 μm square Si wire waveguides to single mode fibres," *Electron. Lett.*, vol. 38, no. 25, pp. 1669–1670, Dec. 2002.
[41] P. Dong, W. Qian, H. Liang, R. Shafiiha, N.-N. Feng, D. Feng, X. Zheng, A. V Krishnamoorthy, and M. Asghari, "Low power and compact reconfigurable multiplexing devices based on silicon microring resonators," *Opt. Exp.*, vol. 18, no. 10, pp. 9852–9858, May 2010.
[42] A. Atabaki, E. Shah Hosseini, A. Eftekhar, S. Yegnanarayanan, and A. Adibi, "Optimization of metallic microheaters for high-speed reconfigurable silicon photonics," *Opt. Exp.*, vol. 18, no. 17, pp. 18 312–18 323, Aug. 2010.
[43] M. R. Watts, J. Sun, C. DeRose, D. C. Trotter, R. W. Young, and G. N. Nielson, "Adiabatic thermo-optic Mach–Zehnder switch," *Opt. Lett.*, vol. 38, no. 5, pp. 733–735, Mar. 2013.